AIP Applied Physics Letters

# Quantitative phase retrieval in transmission hard x-ray microscope

Gung-Chian Yin, Fu-Rong Chen, Yeukuang Hwu, Han-Ping D. Shieh, and Keng S. Liang

Citation: Applied Physics Letters **90**, 181118 (2007); doi: 10.1063/1.2724066
View online: http://dx.doi.org/10.1063/1.2724066
View Table of Contents: http://scitation.aip.org/content/aip/journal/apl/90/18?ver=pdfcov
Published by the AIP Publishing



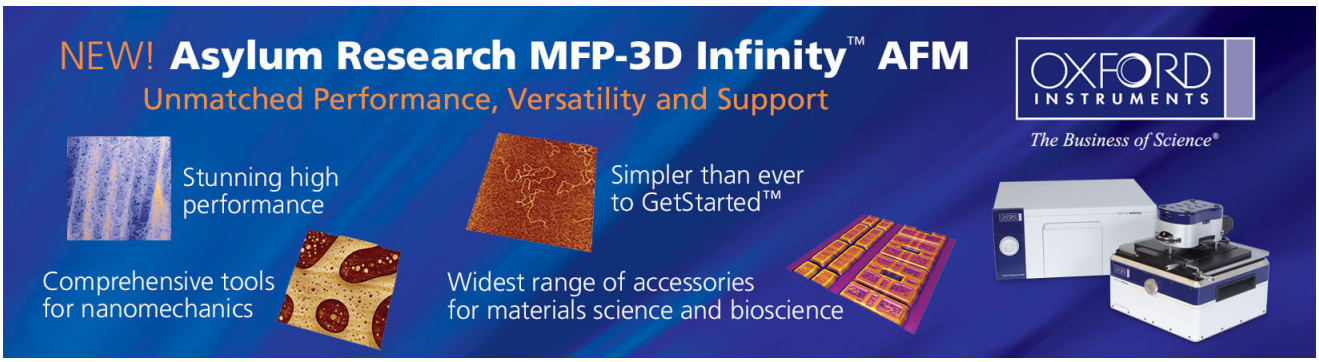

# Quantitative phase retrieval in transmission hard x-ray microscope

Gung-Chian Yin
*National Synchrotron Radiation Research Center, 101 Hsin-Ann Road, Hsinchu 30076, Taiwan; Department of Photonics, National Chiao Tung University, Hsinchu 300, Taiwan; and Display Institute, National Chiao Tung University, Hsinchu 300, Taiwan*

Fu-Rong Chen[a)]
*Department of Engineering and System Science, National Tsing Hua University, Hsinchu 30076, Taiwan and National Synchrotron Radiation Research Center, 101 Hsin-Ann Road, Hsinchu 30076, Taiwan*

Yeukuang Hwu
*Institute of Physics, Academia Sinica,128 Sec. 2, Nankang, Taipei 115, Taiwan*

Han-Ping D. Shieh
*Department of Photonics, National Chiao Tung University, Hsinchu 300, Taiwan and Display Institute, National Chiao Tung University, Hsinchu 300, Taiwan*

Keng S. Liang
*National Synchrotron Radiation Research Center, 101 Hsin-Ann Road, Hsinchu 30076, Taiwan*

(Received 7 February 2007; accepted 5 March 2007; published online 3 May 2007)

Quantitative phase retrieval with a sub-100-nm resolution is achieved from micrographs of a zone plate based transmission x-ray microscope. A plastic zone plate containing objects of sizes from micrometers down to tens of nanometers is used as a test sample to quantify the retrieved phase. Utilizing the focal serial images in the image plane, the phase information is retrieved quantitatively across the entire range of sizes by combining the transport intensity equation and self-consistent wave propagation methods in this partial coherence system. The study demonstrates a solution to overcome the deficiency encountered in the two phase retrieval approaches. © *2007 American Institute of Physics*. [DOI: 10.1063/1.2724066]

Refractive index imaging technique has emerged as a solution to the otherwise low contrast in imaging biological and polymer materials by x rays. Using imaging processing methods to retrieve quantitative phase information was reported previously for visible light,[1] x-ray radiography,[2,3] and electron microscopy,[4,5] with applicable range typically limited to micrometer size. In this work, the approach is applied in treating images of the zone plate type transmission x-ray microscope (TXM),[6,7] which can be applied to specimens of feature size form micrometers down to tens of nanometers. We have developed a methodology of using, in a complementary fashion, two phase retrieval techniques and demonstrated in high resolution x-ray imaging. A similar study[8] but with different approaches was presented with low resolution x-ray radiography. The study shows that image interpretation is more complicated in TXM than that in in-line lensless phase contrast imaging[2] due to the magnification effect. This approach takes advantage of the strength of the transport intensity equation[2,9,10] (TIE) and the self-consistent wave propagation[4,5] (SCWP) methods. We demonstrate that the retrieved results of our experiments using TXM can be compared directly with simulation.

One way to enhance the phase contrast is to use the Zernike phase contrast method,[11] which utilizes a phase plate in the back focal plane of the objective lens to advance the phase of light unscattered by sample light by $\pi/2$ or $3\pi/2$. This leads to a transformation of sample phase modulations into intensity modulations in the image plane. However, the image intensity recorded with a phase plate contains a mixture of absorption and refractive contributions due to the fact that the phase plate (or ring, for TXM) also acts as an aperture that blocks part of the beam to the image.

To overcome the issues mentioned above, quantitative phase information can be deduced from recorded intensity by several imaging processing algorithms, such as TIE and SCWP.[12] The TIE method deduces from the wave equation directly, where the phase information is encoded in the gradient of the intensities recorded at different distances. On the other hand, the SCWP utilizes the wave propagation between the object and image planes iteratively to converge the phase information with the known intensity support. In general, SCWP is known to retrieve phase more effectively at higher frequency in an image, while TIE works best with an object of larger scale (low frequency). The TIE method was applied to x-ray imaging with parallel illumination[2] and partially temporal coherent source[3] with resolution of several micrometers, while SCWP was applied to an electron microscope at atomic resolution.[4,5] However, the resolution between several micrometers and nanometers with hard x ray is acheived recently by using zone plate lens[6,7] and projection type x-ray microscope.[13]

The high resolution x-ray images were obtained from a TXM whose setup is described in detail in our earlier publications.[6,7] The illumination source of the TXM is the x rays emitted from a superconducting wavelength shifter at beamline 01B of NSRRC.[14] In the setup of this study,[7] the focal length is 27 mm for the energy of 8 keV with a magnification of 45. The focal spot of the condenser lens is $\sim 50\ \mu$m and the convergence angle of the condenser is $\sim 0.18$ mrad. The field of view at the objective plane is $15 \times 15\ \mu\text{m}^2$. The depth of the imaging system is estimated

[a)]Electronic mail: frchen@ess nthu.edu.tw



 

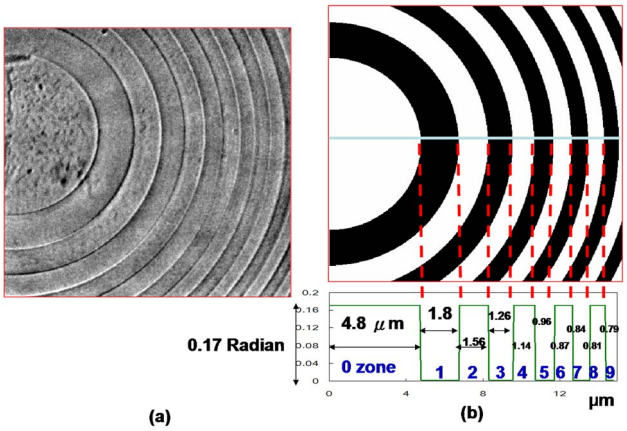


FIG. 1. (Color online) Plastic zone plate is used as the sample. (a) The TXM image of plastic zone plate recorded at zero focus. The illumination aperture already gives rise to an edge fringe, and therefore, the image is not really absorption. (b) A model zone plate, where the white and dark bands correspond to open structures and PMMA structures, respectively. The phase jump between the white and dark bands is calculated to be 0.17 rad. The width of each band is given in the figure. The visible field of view is 15 $\mu$m.

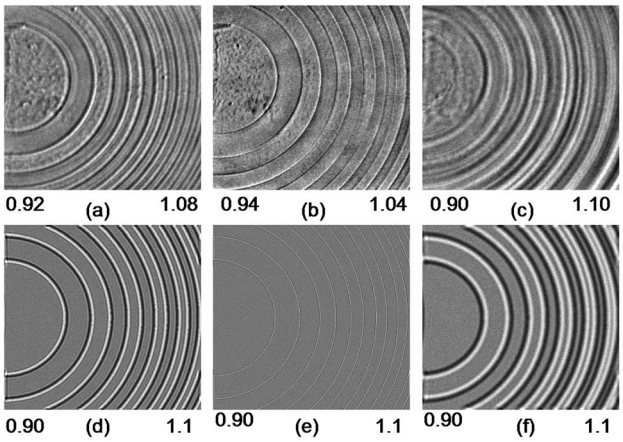


FIG. 2. Experimental and simulated images of TXM. The images in the top row [(a), (b), and (c)] are experimental images taken at positions −400, 20, and 980 $\mu$m from left to right, respectively. The bottom row shows simulated images of the model zone plate at −400, 20, and 980 $\mu$m from left to right [(d), (e), and (f)]. The simulation condition is with the convergent angle $\alpha=1.8\times10^{-4}$ with 2% noise. The values at the bottom of the image are the maximum and minimum of the image.

to be ~80 $\mu$m. By moving the sample along the x-ray propagation direction, a series of defocus series images can be recorded. This sequence is equivalent to the sequence that would be obtained by changing the distance of the detector plane with a multiplication factor $M^2$, where $M$ is the magnification of the TXM, if the defocus distance is small compared to object distance and image distance.

A plastic zone plate was used as a test sample for quantitative phase imaging. The plastic structures are made of 1 $\mu$m thick polymethyl methacrylate (PMMA) ($\delta=-4.18\times10^{-6}$ and $\beta=9.22\times10^{-9}$ at 8 keV) (Ref. 15) on a 0.5 $\mu$m thick silicon nitride. This test zone plate was used as the mold to fabricate gold zone plates, thus there is no PMMA at the center of the plastic zone plate. The phase shift introduced by the PMMA structures is 0.17 rad, calculated by $\varphi=2\pi(\delta d/\lambda)$, where the $\varphi$ is the phase difference, $d$ is the thickness of PMMA, and $\lambda$ is the x-ray wavelength (0.155 nm at 8 keV).

A set of 70 defocus images of the test plastic zone plate was taken with a defocus step of 20 $\mu$m, ranging from −400 to +980 $\mu$m compared to the focused images.[12] The exposure time was 2 min for each image. An x-ray image of this zone plate recorded at focus is shown in Fig. 1(a), which was recorded at the focus position. The defocus images were aligned and normalized against background taken without specimen. In order to quantitatively analyze the retrieved phase from the experimental images, we compared the retrieved phase with that from simulated images of a model zone plate. The model zone plate, shown in Fig. 1(b), has the same dimension as the measured zone plate. The phase jump between the white (air gaps) and dark (the PMMA) bands is set at 0.17 rad.

Three experimental images recorded at the distances of −400, 20, and 980 $\mu$m are shown as examples in Figs. 2(a)–2(c), in which the resulting Fresnel fringes from defocus can be clearly observed. As shown in Figs. 2(d)–2(f), the Fresnel fringes in the simulated images of the same optical conditions are in good agreement with experimental images. 2% of noise in root-mean-square (rms) value was added in the simulated images to facilitate the visual comparison.

Both TIE and SCWP are algorithms to retrieve the phase from a series of recorded intensities of image planes located at equal distance. The SCWP retrieves the phase by an iterative algorithm that replaces the modulus of the propagated wave at each image plane by the measured intensities. The TIE solves the phase $\varphi$ using the gradient of recorded intensities for different distances. The TIE equation is given below.

$$\varphi=\frac{-1}{4\pi^2}\Im^{-1}\left\{\frac{1}{H^2}\Im\left\{\left(-\left(\frac{1}{I_0}\right)k\frac{\partial I}{\partial Z}+\nabla\left(\frac{1}{I_0}\right)\right)\cdot\nabla\left(\frac{-1}{4\pi^2}\Im^{-1}\left\{\frac{1}{H^2}\Im\left\{-k\frac{\partial I}{\partial Z}\right\}\right\}\right)\right\}\right\}, \quad (1)$$

where $H$ is the reciprocal lattice vector, $k$ is the wave vector

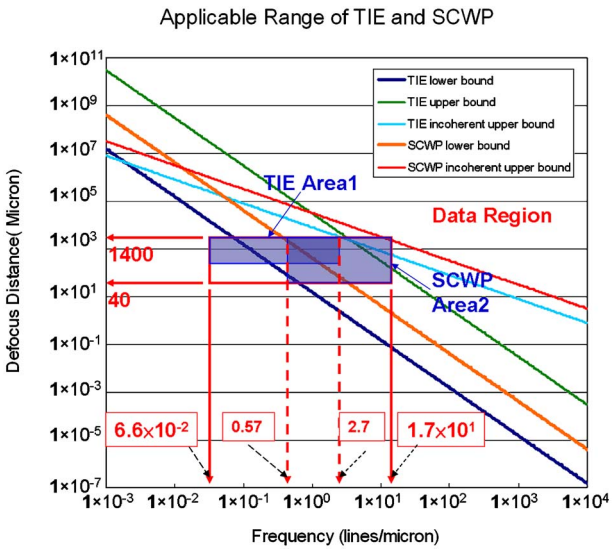


FIG. 3. (Color online) For SCWP, the upper bound is set by the spatial incoherence, depicted as a red line, and the lower bound is set by the phase factor in the propagator $\pi\lambda\Delta f H^2$, depicted as a cyan line, where $\lambda$ is the wavelength and $\Delta f$ is the focal distance. For the TIE, the lower bound is determined by the noise, shown as a dark blue line, while the spatial incoherence, shown as the cyan line, and the separation of image planes are responsible for the upper bounds, shown as the green lines; these lines are given by Ref. 16.

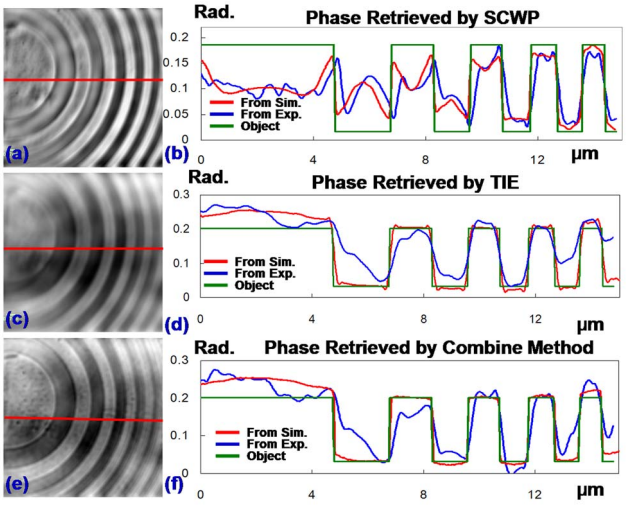


FIG. 4. (Color online) Results of three phase retrieval methods. (a) and (b), the image and the line plots of the phase retrieved by SCWP. (c) and (d), the image and the line plots of the phase retrieved by TIE. (e) and (f), the image and the line plots of the phase retrieved by the combined method. For the combined method, the retrieved phase image by TIE, as shown in (c), from ±400 $\mu$m experimental image pairs was used as an initial solution for SCWP. The red and blue lines are the plots of the retrieved phase using the simulated and experimental images, respectively. The green plot is the ideal object phase from the plastic zone plate.

and is equal to $2\pi/\lambda$, $I_0$ is the intensity at position of zero focus, and $\mathfrak{I}$ and $\mathfrak{I}^{-1}$ are the Fourier and inverse Fourier transformations. The $\partial I/\partial z$ is the gradient of the intensity. The gradient of intensity is usually determined from image pairs symmetrically located at equal distance from the zero focus.

The applicability of TIE and SCWP in terms of the focal distance as a function of object size is discussed in detail in a previous paper,[16] and the applicable parameter space for each method is shown in Fig. 3. Note that those boundary lines in Fig. 3, however, depend on the presence of noise and may vary in different experimental cases. The blue boxes denoted as TIE area 1 and SCWP area 2 in Fig. 3 are the estimated applicable range for TIE and SCWP for this experiment. The horizontal axis in Fig. 3 is the spatial frequency of the object, and the vertical axis is the defocus distance. The spatial frequency range of the type recorded ranges between $\sim 6.6\times 10^{-2}$ lines/$\mu$m, the inverse of the 15 $\mu$m field of view, and $1.7\times 10^{1}$ lines/$\mu$m, the maximum frequency for a $512\times 512$ pixel image. It is obvious that TIE or SCWP alone is not sufficient to fully cover the whole frequency range. Thus, the strategy of phase retrieval is to use the TIE for data of large distance to have better low frequency response and then use the SCWP for data of short distance to have better high frequency response. Based on the estimated applicable range shown in Fig. 3, the TIE has a better response in the frequency range below 2.7 lines/$\mu$m, which is from the defocus distance of 1400(±700) $\mu$m; which is confirmed by the simulation. The low frequency of SCWP is around 0.57 line/$\mu$m; the result is confirmed by both simulation and experiment.

The retrieved phase by the TIE using experimental image pairs at ±400 $\mu$m served as an initial solution for SCWP to refine. The results of the three methods, SCWP, TIE, and combined methods, are shown in Fig. 4. The red and blue lines are the line plots of the retrieved phase from the simulated and experimental images. The green plot is the ideal object phase from the model zone plate. In SCWP, the experiment result agrees well with simulation data and has lower response and lower frequency. In TIE, the result has better response at low frequency, and in Fig. 4(c), the details of the image are blurred because of the lower response at high frequency. The result of the combined methods is shown in Figs. 4(e) and 4(f). The SCWP therefore improves the phase recovery at higher frequency, while it keeps the phase unaltered at lower frequency. The signal of higher frequency can also be seen from the appearance of the fine features of nanoscale particles.

In conclusion, we demonstrate that the phase retrieval methods of TIE and SCWP can be applied to the zone plate type transmission x-ray microscope at sub-100-nm resolution. The quantitative phase of a test plastic zone plate containing an object size across the applicability ranges of TIE and SCWP can be deduced efficiently using the combination of TIE and SCWP.

The authors thank Mau-Tsu Tang and Yang-Feng Song of NSRRC for help. G.-C.Y. thanks Michael Feser and Wenbing Yun of Xradia Inc. for valuable discussion.

[1] A. Barty, K. A. Nugent, D. Paganin, and A. Roberts, Opt. Lett. **23**, 817 (1998).
[2] K. A. Nugent, T. E. Gureyev, D. F. Cookson, D. Paganin, and Z. Barnea, Phys. Rev. Lett. **77**, 2961 (1996).
[3] D. Paganin and K. A. Nugent, Phys. Rev. Lett. **80**, 2586 (1998).
[4] L. J. Allen, W. McBride, N. L. O'Leary, and M. P. Oxley, Ultramicroscopy **100**, 91 (2004).
[5] W. Hsieh, F. Chen, J. Kai, and A. I. Kirkland, Ultramicroscopy **98**, 99 (2004).
[6] G. Yin, F. W. Duewer, M. Feser, M. Tang, Y. Song, F. Chen, W. Yun, H. D. Shieh, and K. S. Liang, Appl. Phys. Lett. **89**, 221122 (2006).
[7] G. Yin, M. Tang, Y. Song, F. Chen, F. W. Duewer, W. Yun, C. Ko, H. D. Shieh, and K. S. Liang, Appl. Phys. Lett. **88**, 241115 (2006).
[8] B. D. Arhatari, A. P. Mancuso, A. G. Peele, and K. A. Nugent, Rev. Sci. Instrum. **75**, 5271 (2004).
[9] M. R. Teague, J. Opt. Soc. Am. **73**, 1434 (1983).
[10] T. E. Gureyev, A. Roberts, and K. A. Nugent, J. Opt. Soc. Am. A **12**, 1932 (1995).
[11] F. Zernike, Physica (Amsterdam) **9**, 686 (1942).
[12] See EPAPS Document No. E-APPLAB-90-062715 for TIEandSCWP.pdf, experiment.avi, and simulation.avi. This document can be reached via a direct link in the online article's HTML reference section or via the EPAPS homepage (http://www.aip.org/pubserves/epaps.html).
[13] S. C. Mayo, T. J. Davis, T. E. Gureyev, P. R. Miller, D. Paganin, A. Pogany, A. W. Stevenson, and S. W. Wilkins, Opt. Express **11**, 2289 (2003).
[14] National Synchrotron Radiation Research Center http://srrcbl.nsrrc.org.tw/
[15] Center of X-ray Optics http://www-cxro.lbl.gov/
[16] A. V. Martin, F.-R. Chen, W.-K. Hsieh, J.-J. Kai, S. D. Findlay, and L. J. Allen, Ultramicroscopy **106**, 914 (2006).